Int. J. Radiation Oncology Biol. Phys., Vol. 49, No. 4, pp. 1097–1108, 2001

0360-3016/01/$–see front matter

PII S0360-3016(00)01460-7

BIOLOGY CONTRIBUTION

TUMOR OXIMETRY: DEMONSTRATION OF AN ENHANCED DYNAMIC MAPPING PROCEDURE USING FLUORINE-19 ECHO PLANAR MAGNETIC RESONANCE IMAGING IN THE DUNNING PROSTATE R3327-AT1 RAT TUMOR

SANDEEP HUNJAN, PH.D., DAWEN ZHAO, M.D., PH.D., ANCA CONSTANTINESCU, PH.D., ERIC W. HAHN, PH.D., PETER P. ANTICH, PH.D., D.SC., AND RALPH P. MASON, PH.D.

Advanced Radiological Sciences, Department of Radiology, University of Texas Southwestern Medical Center, Dallas, TX

Purpose: We have developed an enhanced approach to measuring regional oxygen tension (pO_2) dynamics in tumors. The technique is demonstrated in a group of 8 Dunning prostate rat tumors (R3327-AT1) with respect to respiratory challenge.

Methods and Materials: Hexafluorobenzene was injected directly into the tumors of anesthetized rats. ^{19}F nuclear magnetic resonance echo planar imaging relaxometry was performed to obtain maps of regional tumor oxygenation under baseline conditions and when the inhaled gas was changed to oxygen or carbogen.

Results: Sequential pO_2 maps required 8 min, with a typical precision of 1–3 torr at 30–100 individual regions across a tumor. When rats breathed 33% oxygen, distinct heterogeneity was observed for baseline oxygenation in each tumor with pO_2 values ranging from hypoxic to greater than 100 torr. Larger tumors showed significantly lower baseline pO_2. Respiratory challenge with oxygen or carbogen produced significant increases in tumor oxygenation with a close correlation between the response to each gas at individual locations. Regions of both small and large tumors responded to respiratory challenge, but the rate was generally much faster in initially well-oxygenated regions.

Conclusions: Regional pO_2 was assessed quantitatively and the response of multiple individual tumor regions observed simultaneously with respect to interventions.

Hypoxia, Fluorine magnetic resonance imaging, Oxygen, Carbogen, Tumor.

INTRODUCTION

Increasingly, there is clinical evidence for the value of tumor oxygen tension (pO_2) as a prognostic indicator for survival of patients (1–4). Furthermore, it has long been appreciated that the efficacy of many therapeutic approaches to tumor treatment is modulated by oxygen tension: in particular, radiotherapy (5), photodynamic therapy (6), and certain drugs (7) are less effective in the absence of oxygen. Many adjuvant interventions have been tested to manipulate tumor oxygenation, e.g., hyperbaric oxygen; but few trials have shown significant efficacy (8). This has often been attributed to the inability to identify those patients who would benefit. Historically, it was not possible to reliably monitor tumor oxygenation. However, the development of novel therapies, such as application of bioreductive drugs (9–11), has generated new impetus to assess tumor oxygenation.

Given the importance of oxygen, many techniques for measuring pO_2 have been developed (12). Each method has unique strengths, but, hitherto, the Eppendorf electrode system was the only one to have found widespread application for quantitative examination of tumor pO_2, in both small-animal research and clinical trials (1–4, 13, 14). Several clinical studies have now shown prognostic value for such polarographic measurements in primary tumors, although there is debate about the most useful parameter e.g., median pO_2 (1) or fraction of measurements less than 5 torr (2). However, extensive tumor sampling with electrodes is highly invasive and does not allow longitudinal studies of dynamic changes in specific tumor regions.

We recently demonstrated a novel approach to monitoring tumor oxygenation based on ^{19}F NMR of the reporter molecular hexafluorobenzene (HFB) following direct intra-

Reprint requests to: Ralph P. Mason, Ph.D., C. Chem., Department of Radiology, University of Texas Southwestern Medical Center, 5323 Harry Hines Blvd., Dallas, TX 75390-9058. E-mail: Ralph.Mason@UTSouthwestern.edu

Presented in part at the International Society of Magnetic Resonance in Medicine Meeting, St. Louis, MO, November 1998, and the AACR Workshop on Molecular Determinants of Cancer Treatment, Whistler, BC, March 1999.

This work was supported in part by The American Cancer Society (RPG-97-116-010CCE) and NIH RO1 CA 79515-01. NMR experiments were performed at the Mary Nell and Ralph B. Rogers MR Center, an NIH BRTP Facility P41-RR02584.

Acknowledgments—We are grateful to Drs. Mark Jeffrey and Evelyn Babcock for maintaining the MR systems and Yulin Song for technical assistance.

Accepted for publication 22 September 2000.

tumoral (i.t.) injection. Initially, we demonstrated the ability to interrogate single-tumor regions using ^{19}F NMR spectroscopy, and we were able to show significantly different responses of specific regions, which correlated with baseline pO_2 (15, 16). By applying Echo Planar Imaging (EPI) we were able to simultaneously examine multiple specific locations within a tumor using a procedure we have dubbed FREDOM (Fluorocarbon Relaxometry using Echo planar imaging for Dynamic Oxygen Mapping). This allowed us to simultaneously interrogate well- and poorly oxygenated regions with respect to a single intervention and appreciate both baseline heterogeneity and differences in response within a single tumor (17, 18). Typically, we could interrogate approximately 20 individual locations (each $\sim$ 1.25 mm^2) in any particular pO_2 map and consistently follow dynamic changes in approximately 10 locations with a temporal resolution approximately 20 min and precision of approximately 5 torr during an intervention. Significantly, the pO_2 values were not different from those obtained using the Eppendorf Histograph (18).

We have now developed an enhanced data acquisition protocol, ARDVARC (Alternated Relaxation Delays with Variable Acquisitions to Reduce Clearance effects), which dramatically improves the efficiency and precision of the procedure. Initial tests with spectroscopy demonstrated enhanced quality of relaxation curves and enhanced precision in pO_2 estimates (16). By implementing this procedure with echo planar imaging, we have now shown the ability to consistently interrogate 30–100 individual tumor regions simultaneously at 8-min intervals. Specifically, we have examined the influence of respiratory challenge using oxygen or carbogen on the oxygenation of transplanted rat prostate tumors.

METHODS AND MATERIALS

Calibration

A phantom (17) was created to evaluate the relationship between pO_2 and the spin lattice relaxation rate, R1 (= 1/T1). 125 μL HFB (Lancaster, Gainesville, FL) was added to each of 4 gas tight NMR tubes (Wilmad Glass Co., Buena, NJ) together with 0.5 mL water and saturated by bubbling at 37°C with carbon dioxide, 1% oxygen (balance nitrogen), 9.8% oxygen (balance nitrogen), or air, respectively. Tubes were sealed and the phantom maintained at 37°C using a water bath. A 3-cm single turn solenoid coil was placed around the phantom, which was placed in an Omega CSI 4.7 Tesla horizontal bore magnet system with actively shielded gradients. With 32 data points in both the phase encode and readout dimensions the typical 40 $\times$ 40 mm field of view provided 1.25 mm in plane resolution. The FREDOM protocol used ^{19}F pulse burst saturation recovery (PBSR) EPI relaxometry of the HFB with a single spin echo EPI sequence with blipped phase encoding (MBEST), as described previously (17). The PBSR preparation sequence was followed by a relaxation recovery delay, τ, ranging from 150 ms to 90 s prior to the EPI sequence. To improve the quality of the data, however, we introduced the ARDVARC acquisition protocol (16), which has two features: (*1*) long and short delays alternated to minimize any systematic variations, which could occur during the acquisition, and (*2*) variable numbers of signal averages obtained to enhance the signal to noise ratio at the low amplitude points, e.g., 12 averages at 150 ms and a single acquisition for 90 s. The total experiment time was 6.5 min., as for the analogous spectroscopic NMR approach. The spin-lattice relaxation rate was estimated on a voxel by voxel basis using a 3-parameter mono-exponential function and the Levenberg–Marquardt least squares algorithm, which provided estimates of T1, signal amplitude, signal origin, T1 error, and goodness of fit (19). Filters were applied to reject poor quality data and out of phase ghost artifacts: specifically, acceptable voxels had T1error less than 2 s; ratio T1error/T1 less than 50% and SNR greater than 15. Based on these data, the relationship $R1 = a + bpO_2$ was established by linear regression analysis of the amplitude squared weighted mean values for each gas (Statview, SAS Institute, Cary, NC).

Tumor model

Dunning prostate adenocarcinoma R3327-AT1 was implanted in a skin pedicle on the foreback of a male Copenhagen rat ($\sim$250 g, $n = 8$), as described in detail previously (20). Tumors were divided into two groups and allowed to grow to about 16 mm or greater than 20 mm diameter ($\sim$2 or $>$3.5 cm^3 volume). For MR investigations: each rat was given 200 μL ketamine hydrochloride (100 mg/mL; Aveco, Fort Dodge, IA) i.m., as a relaxant. The rat was maintained under general gaseous anesthesia with 33% inhaled O_2 (0.3 dm^3/min O_2, 0.6 dm^3/min N_2O, and 0.5% methoxyflurane (Pitmann-Moore, Washington Crossing, NJ) using a small-animal anesthesia unit. Hexafluorobenzene (45 μL) was injected directly into the tumor (i.t.) using a Hamilton syringe (Reno, NV) with a custom-made fine sharp needle (32 gauge). The animal was placed on its side in a cradle with a thermal blanket to maintain body temperature. A fiber optic probe was inserted rectally to monitor core temperature.

A size-matched tunable ($^1H/^{19}F$) single-turn solenoid coil was placed around the tumor. Shimming was performed on the ^1H signal (200.1 MHz) of the tissue water to a typical linewidth of 120 Hz. Proton images were obtained for anatomic reference using a three-dimensional (3D) spin-echo sequence. Imaging parameters were: repetition time (TR) = 150 ms, echo time (TE) = 80 ms, pulse width $\pi/2 = 32$ μs with 128 $\times$ 64 $\times$ 8 data points over the 32-mm field of view in plane, and 32-mm thickness, providing 250 μm $\times$ 500 μm $\times$ 4 mm digital resolution. Two transients were acquired at each phase encoding increment giving a total acquisition time of 2.5 min. The coil was retuned in place to 188.3 MHz and corresponding ^{19}F images were obtained as a 3D data set with 128 $\times$ 32 $\times$ 8 data points and gradients compensated for the difference in gyromagnetic ratios, yielding 250 μm $\times$ 1 mm $\times$ 4 mm resolution. A

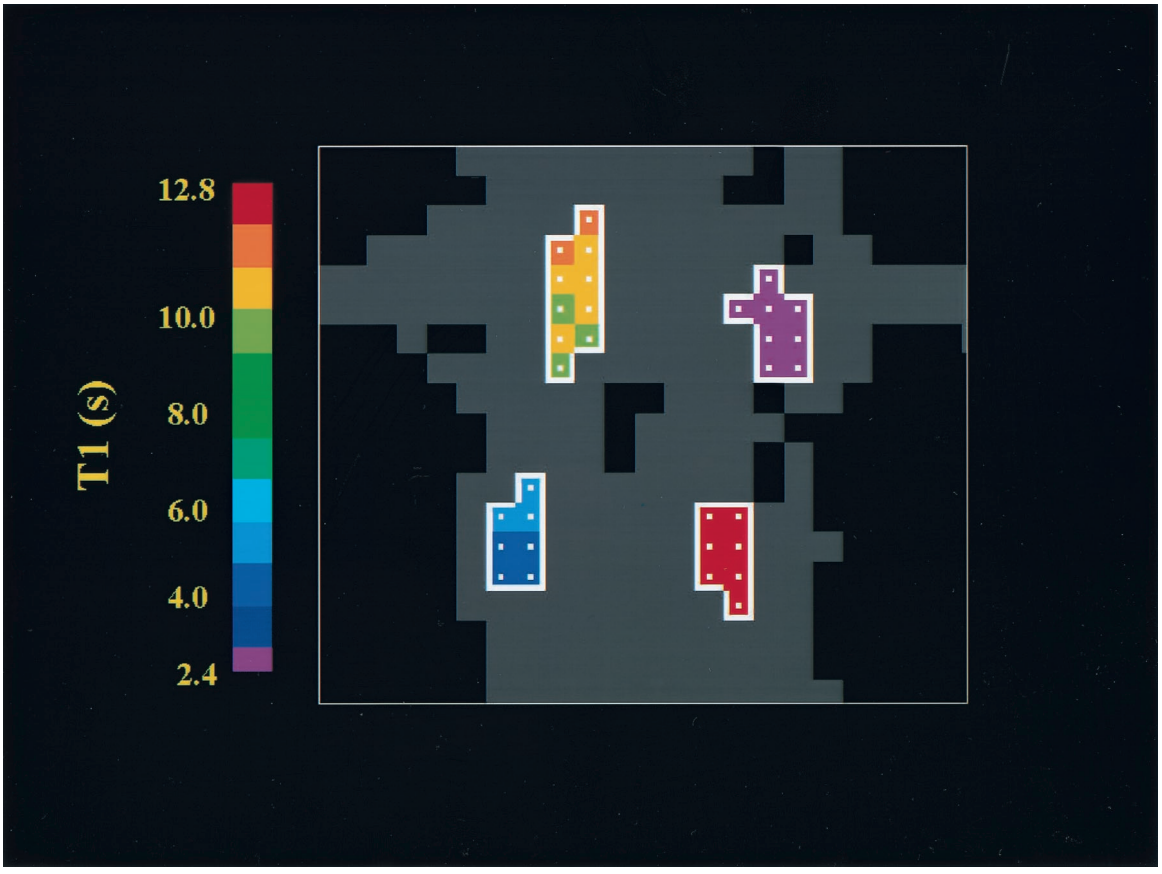

Fig. 1. Representation of the ^{19}F NMR T1 values observed in a 4-vial phantom at 37°C, where vials had been saturated with carbon dioxide (bottom right), 1% oxygen (top left), 9.8% oxygen (bottom left), or air (top right), respectively. Filters were applied to select the most reliable data based on T1 error and the fully relaxed signal amplitude.

driven-equilibrium sequence was applied with TR = 150 ms, TE = 8 ms, $\pi/2$ (33 μs) excitation pulse and 16 transients at each increment giving a total accumulation time of 10 min. for the 3D data set. These ^{19}F images revealed the distribution of the HFB. Data were processed using sine-bell apodization and zero filling in the first phase encode dimension.

Tumor oximetry

All eight rats were subjected to respiratory challenge with oxygen. While the rat inhaled 33% O_2, 3 consecutive baseline pO_2 maps were generated (at 8-min intervals), as described for the phantom above using the FREDOM procedure. The inhaled gas was then altered to 100% oxygen (though methoxyflurane was held constant at 0.5%), and relaxation measurements (4 × 8 min) were immediately performed. The gas was switched back to the initial baseline state for a further four determinations. For 3 rats, the gas was further altered to carbogen (four measurements) and again back to baseline (33% O_2). Statistics are reported as mean ± SE (standard error of the mean), median, IPR (interpercentile range, 10–90%) and significance of changes in oxygenation was assessed using analysis of variance (ANOVA) on the basis of Fisher PLSD (Statview).

RESULTS

Application of the ARDVARC data acquisition protocol provides considerably improved precision in estimating the spin lattice relaxation rate of HFB, and, hence, pO_2. Specifically, the enhanced signal to noise ratio (SNR) for short τ low-intensity data points provides superior curve fitting, as demonstrated previously for the analogous spectroscopic experiment (16). Thus, we have created a refined calibration curve relating spin lattice relaxation rate, R1 (=1/T1), to pO_2. A representation of the T1 values observed in the phantom is shown in Fig. 1. Figure 2 shows the linear regression curve, based on the amplitude squared weighted mean $R1$ values, which indicated a relationship $R1\ (s^{-1}) = 0.0835\ (\pm\ 0.0010) + 0.001876\ (\pm\ 0.000009) \times pO_2$ (torr), $r^2 > 0.999$, thus, $pO_2 = (R1 - 0.0835)/0.001876$ at 37°C.

Following intratumoral injection, HFB distribution was readily observed by traditional ^{19}F MR imaging. Figure 3 shows 4 consecutive slices from a 3D image data set of a representative tumor. Overlay of the ^{19}F MR images on the corresponding proton images shows the discrete distribution of HFB in the tumor. In this case, HFB was predominately placed near the tumor periphery. For the series of EPI relaxation data sets, typically, approximately 100–300 vox-

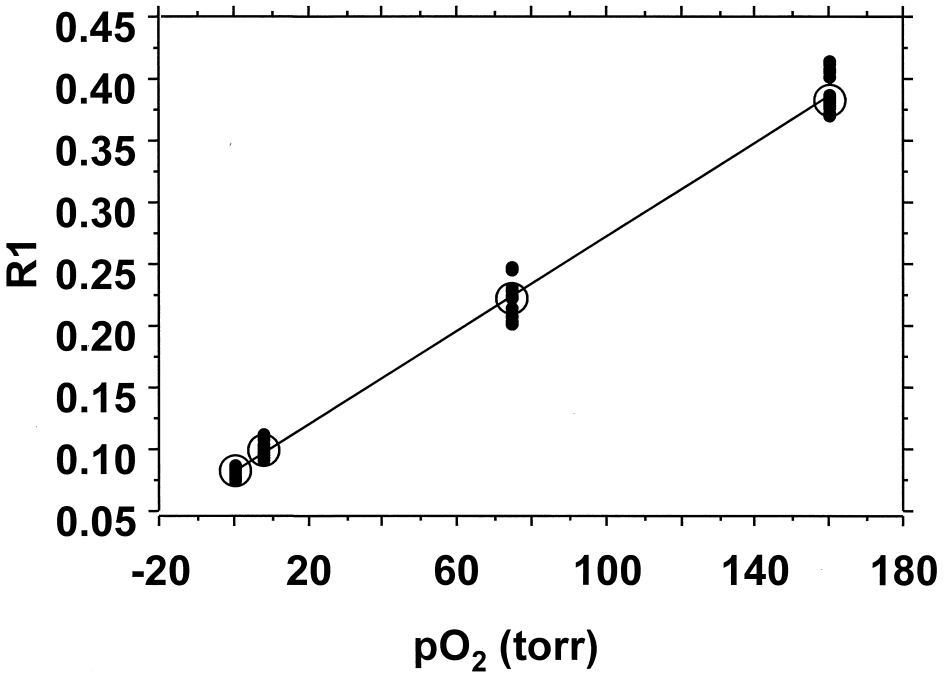

Fig. 2. Linear regression based on the amplitude squared weighted means (open circle) of the respective vials in Fig. 1 indicated $R1$ (s^{-1}) = 0.0835 (± 0.0010) + 0.001876 (± 0.000009)×pO_2 (torr), $r^2 > 0.999$, where $R1 = 1/T1$. Solid circle represents R1 values of the individual voxels.

els provided an R1 fit, and potential pO_2 value using the equation determined above. However, this included voxels physically outside the tumor, i.e., noise and out-of-phase ghost artifacts. By considering the traditional ^1H and ^{19}F images, which revealed the distribution of HFB within the tumor, a mask was applied to restrict the distribution of acceptable voxels. In addition, data were rejected if the T1 error exceeded 3 s. Generally, those voxels with greater signal intensity gave the best curve-fit data and most precise T1 (*viz*. pO_2) values (Fig. 4a and b). Typically, ~40 voxels from each pO_2 map were defined as reliable data for a respiratory challenge sequence (Fig. 4). In this tumor, there was considerable heterogeneity in baseline pO_2 with one region being relatively poorly oxygenated. Repeat measurements every 8 min under baseline conditions demonstrated relative stability of tumor oxygenation (Fig. 4c and d). Considerable increases in regional pO_2 were found for those regions initially well oxygenated after the rat had inhaled 100% oxygen for 20 mins (Fig. 4e). In contrast, those regions initially poorly oxygenated showed little change. Fig. 4f shows a tendency to return to baseline oxygenation after inhaled gas was returned to 33% O_2.

For the group of 8 tumors ranging in size from 1.4 to 5.7 cm^3 (mean, 3.2 cm^3), 3 repeat measurements interrogating

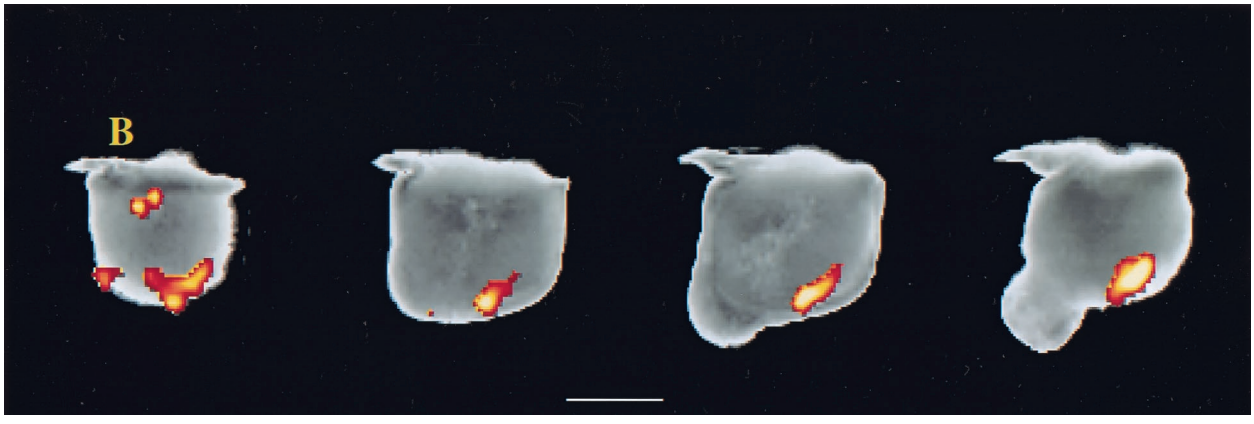

Fig. 3. Magnetic resonance (MR) images from 3D (three-dimensional) data set showing the distribution of hexafluorobenzene (HFB) (45 μL) in an AT1 pedicle tumor (2.0 cm^3). Overlay of ^{19}F MR signal density on the ^1H MR images achieved using NIH image software (yellow is higher intensity than red). "B" indicates point of attachment of pedicle to back of rat. Bar represents 1 cm.

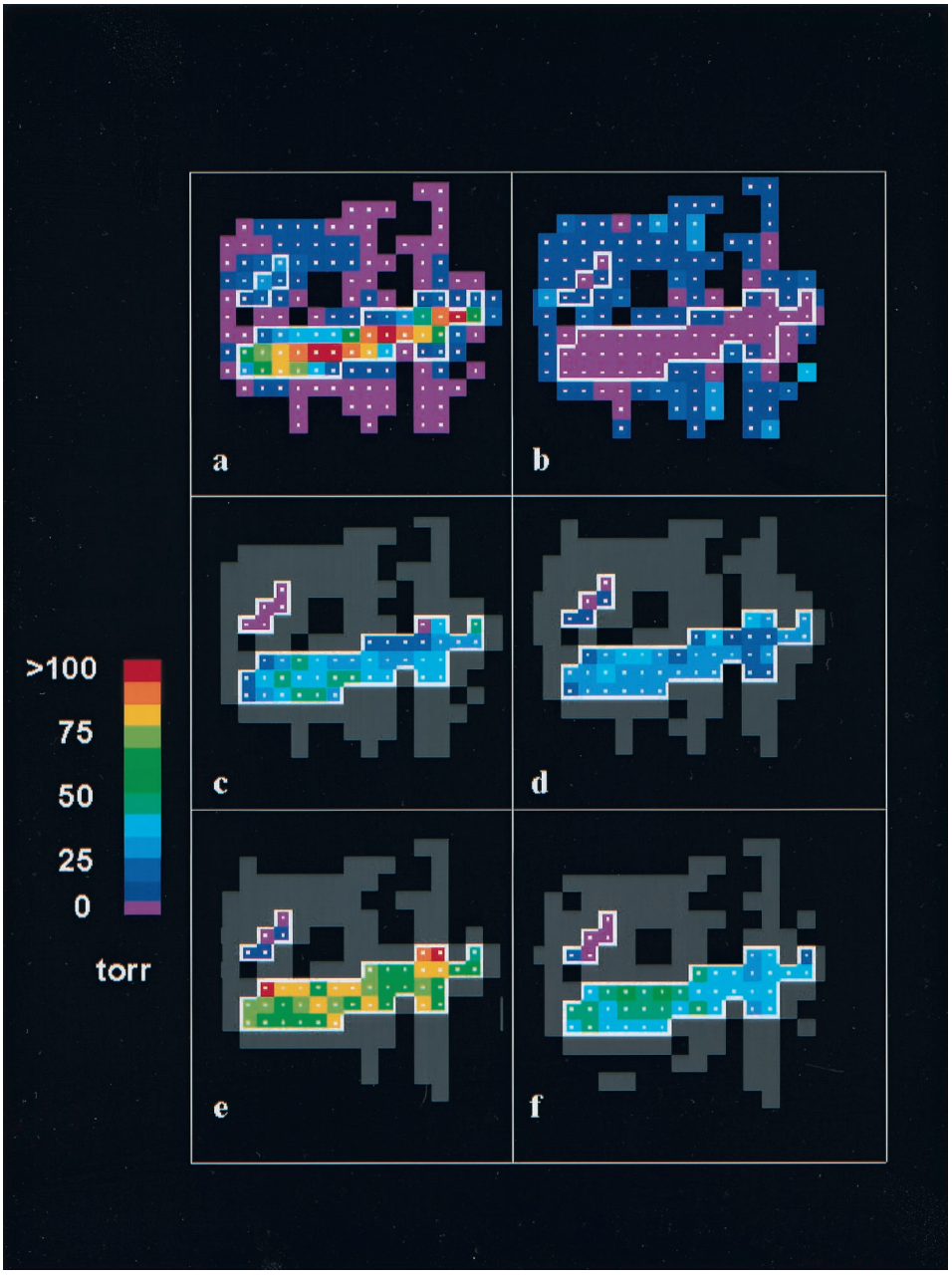

Fig. 4. ^{19}F MR EPI maps of hexfluorobenzene (HFB) in AT1 tumor shown in Fig. 3. (a) Signal amplitude indicating distribution of HFB; (b) T1 error map, showing that higher SNR is generally associated with smaller errors and, hence, more precise data; (c–f) pO_2 maps with respect to respiratory challenge. The center maps (c, d) were obtained while the rat breathed 33% FO_2 (fraction of inhaled oxygen) and indicate a stable baseline. Two distinct regions were apparent, the larger having 37 relatively well-oxygenated voxels and the smaller region 5 poorly oxygenated voxels. Upon switching the inhaled gas to oxygen (map e), the larger region showed distinct increase in pO_2, whereas the relatively hypoxic region showed minimal change. Return to 33% FO_2 (map f) shows that the higher pO_2 values tended to return to the original baseline levels.

about 500 separate tumor regions (voxels) showed mean $pO_2 \pm$ SE (median in parentheses) = 31.4 ± 1.1 (26.9), 31.3 ± 1.1 (25.8), and 34.9 ± 1.2 (31.1) torr, respectively, indicating no significant differences over 24 min. Overall, combining the three sets of measurements gave mean baseline pO_2 = 32.3 ± 0.7 torr; IPR, 5–116 torr; median, 27.4 torr. Because previous data has indicated size dependence for pO_2 in this tumor line, we divided the tumors into groups based on size. For the 4 smaller tumors, mean pO_2 = 37.2 ± 0.8; IPR, 9–70 torr; and median, 31.7 torr, which was significantly higher ($p < 0.0001$) than for the 4 larger tumors (> 3.5 cm^3) with mean baseline pO_2 = 21.7 ± 1 torr; IPR, −2 to 50 torr; median, 16.7 torr. Data are presented as histograms in Fig. 5, both for baseline and for accompanying respiratory challenge with 100% O_2. Elevated fraction of inhaled O_2 (FO_2) produced a significant

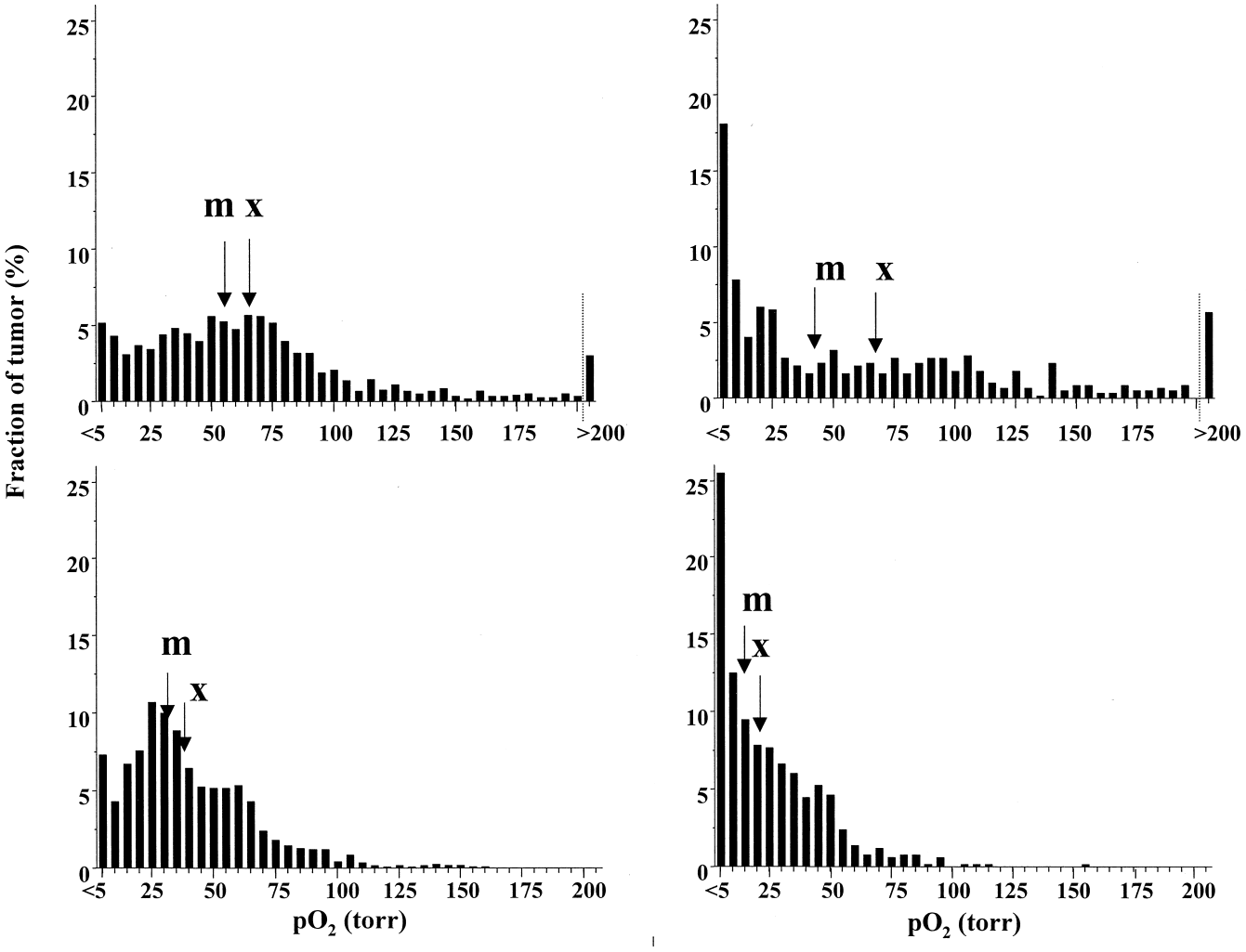

Fig. 5. Histograms of oxygenation based on ^{19}F MR EPI relaxometry for AT1 tumors based on size and inhaled gas. Data have been pooled in bins of 5 torr: the designated values, e.g., 5, 25 torr, indicating the maximum value. Arrows indicate mean pO_2 (x) and median pO_2 (m). Left: Four small tumors (< 3 cm^3), while rats inhaled $FO_2 = 33\%$ (bottom), mean $pO_2 = 37.2 \pm 0.8$, median $pO_2 = 31.7$ torr; and breathing oxygen (top), mean $pO_2 = 66.5 \pm 1.5$ torr, median $pO_2 = 56.7$. Right: Four large tumors (>3.5 cm^3), while rats inhaled $FO_2 = 33\%$ (bottom), mean $pO_2 = 21.7 \pm 1$ torr, median $pO_2 = 16.7$ torr; and breathing oxygen (top), mean $pO_2 = 65.6 \pm 3$ torr, median $pO_2 = 43.4$ torr.

shift in mean pO_2 to 66.2 ± 1.4 torr (median, 54.1 torr; $p < 0.0001$). The small tumors increased to 66.5 ± 1.5 torr; median, 56.7 torr; IPR, 11.4–129 torr; and large tumors increased to mean of 65.6 ± 3 torr; IPR, -0.9 to 166 torr; and median, 43.4 torr. The histograms show pooled data for all measurements while inhaling a given gas, but individual time points may also be compared. For the small tumors, pO_2 changed significantly within 8 min of inhaling oxygen ($p < 0.005$). Upon return to baseline ($FO_2 = 33\%$), changes in pO_2 occurred more slowly, but, by the third or fourth measurement, pO_2 was no longer significantly different from baseline. Similar behavior was observed for the large tumors.

A primary strength of the ^{19}F EPI approach is the ability to follow simultaneously the sequential fate of individual tumor regions. Fig. 6 shows the fate of 6 representative voxels from the tumor shown in Figs. 3 and 4. Within 8 min of increasing the fraction of inhaled O_2, the regions with an initial pO_2 greater than 10 torr had distinct increases in pO_2 ($p < 0.05$). By contrast, the initially poorly oxygenated regions showed no changes for at least 24 min. Two of these regions did show a borderline change for the measurement finishing at 32 min ($p < 0.1$). All changes were reversible upon return to baseline inhaled oxygen.

Correlation between mean baseline pO_2 of each voxel and maximum pO_2 detected in the voxel with 100% oxygen is shown in Fig. 7. As expected because of tumor heterogeneity, the linear regression correlation coefficient is low ($r^2 = 0.3$), but more than 90% of the data lie above the line of unity, and a paired Student's t test showed a significant elevation in pO_2 ($p < 0.001$). More importantly, from a radiobiologic perspective, applying the Student's t test to a group of 80 tumor regions with mean baseline pO_2 less than

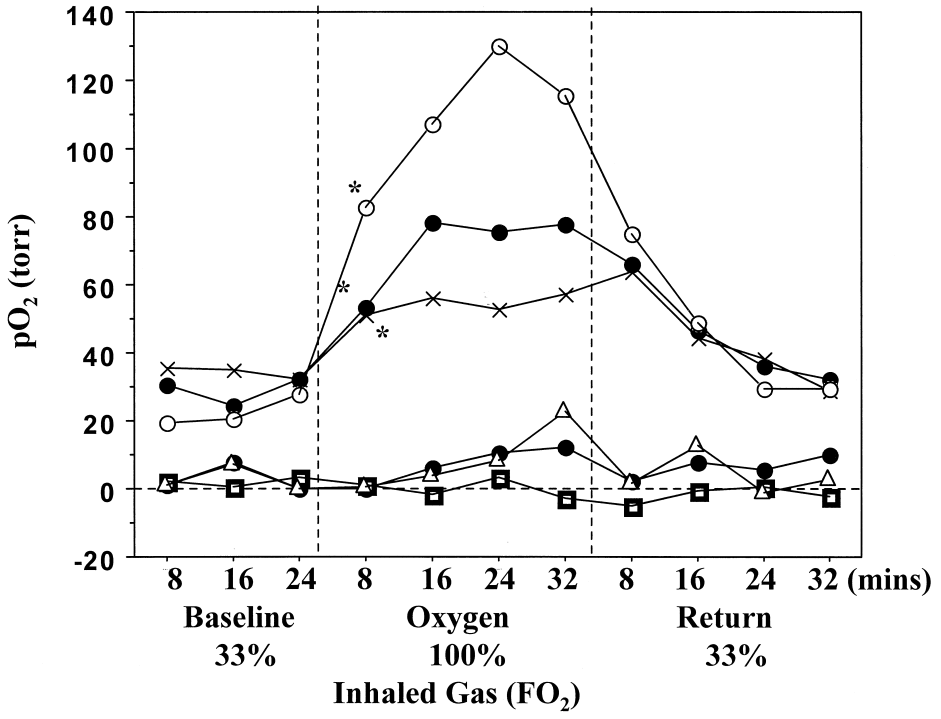

Fig. 6. Variation in pO_2 for 6 representative voxels of the tumor shown in Figs. 3 and 4.

15 torr, indicated that the new pO_2 was significantly elevated ($p < 0.0001$).

Three tumors also underwent subsequent respiratory challenge with carbogen and variation in mean pO_2 for the group is shown in Fig. 8. For this group of tumors, pO_2 was significantly elevated from a baseline value of 46 ± 2 torr to 73 ± 6 torr ($p < 0.0005$; median, 45.0 and 55.7 torr, respectively) within 16 min of switching the inhaled gas from FO_2 33% to FO_2 100%, and pO_2 continued to rise through the subsequent measurements to reach a mean of 103 ± 8 torr (median, 78.6 torr) after 32 min. pO_2 remained significantly elevated for the first two measurements after return to baseline gas, but ultimately (by 32 min) was not significantly different from baseline.

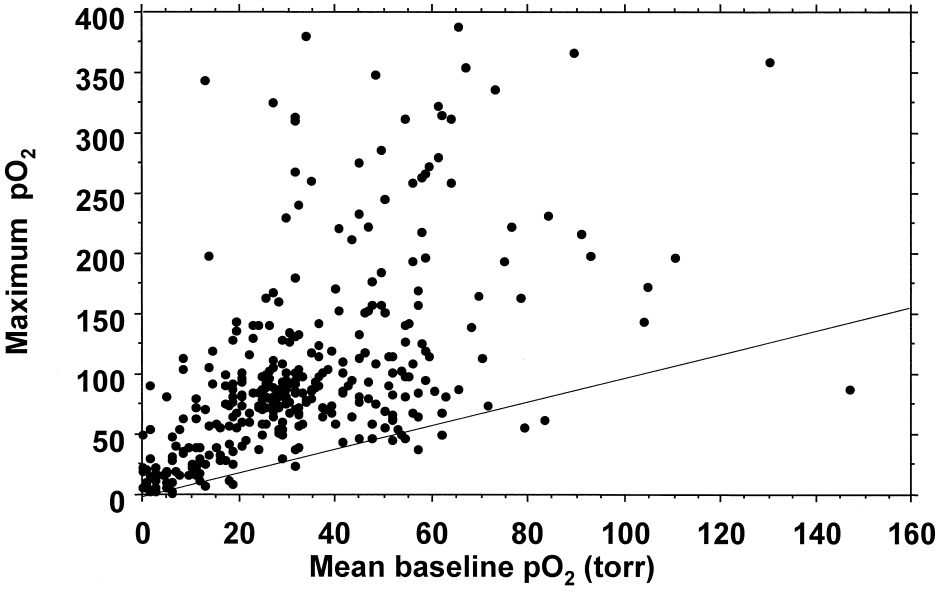

Fig. 7. Correlation between mean baseline pO_2 and maximum pO_2 detected with 100% oxygen. The linear regression correlation coefficient is low ($r^2 = 0.3$), but approximately 90% of data lie above the line of unity, and a paired Student's *t* test shows $p < 0.001$.

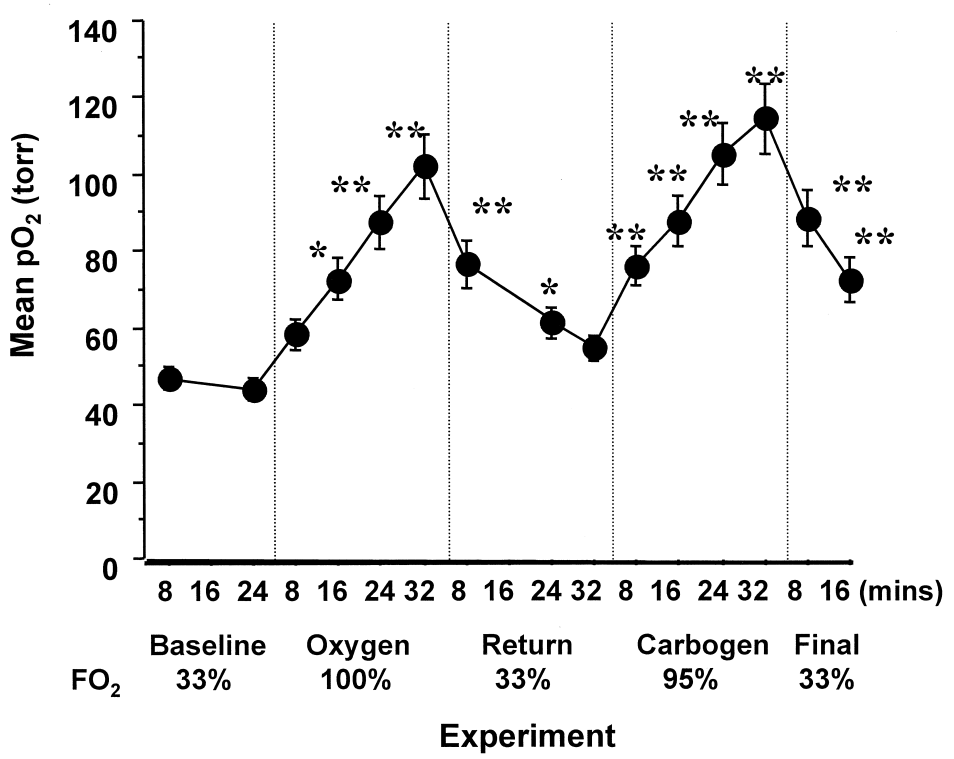

Fig. 8. Variation in mean ± SE pO_2 during respiratory challenge for a group of 3 tumors, in which the same 109 individual voxels were observed on each occasion. *$p < 0.05$; **$p < 0.0001$. Each measurement required about 8 min.

The response curve to carbogen was similar to that for oxygen: the initial increase occurred a little faster, reaching significance within the first 8 min, but, ultimately, the mean $pO_2 = 115 \pm 9$ (median, 86.1 torr) after 32 min was not significantly different from the maximum reached with oxygen. Figure 9 shows a close correlation between the maximum pO_2 achieved in individual tumor regions (voxels) upon breathing carbogen as compared with oxygen ($r^2 > 0.7$). As for oxygen, a paired *t* test showed that the important baseline regions with pO_2 of less than 15 torr increased significantly with carbogen inhalation, but there was no significant difference between the maximum pO_2 achieved with oxygen or carbogen for these initially relatively poorly oxygenated regions.

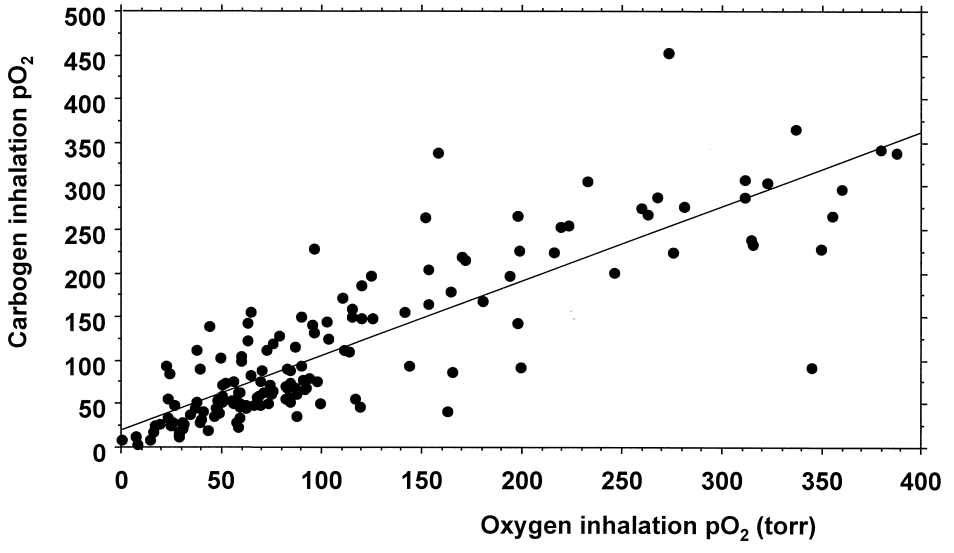

Fig. 9. Correlation between maximum pO_2 detected in each voxel when rat breathed oxygen (FO_2 100%) vs. carbogen ($r^2 > 0.7$).

DISCUSSION

In common with previous studies describing many diverse tumors, and in particular, the R3327-AT1 tumor line (17, 18, 21, 22), we have found considerable intratumoral heterogeneity in the distribution of pO_2 values, ranging from distinctly hypoxic to well oxygenated. As with previous groups of AT1 tumors implanted in the pedicle (18), we have again found significantly lower mean pO_2 in larger tumors (> 3.5 cm^3). This coincides with a general trend toward lower pO_2 with increasing size found in the AT1 implanted i.m. and examined using the histograph (22). In the current series of tumors, we examined predominantly the tumor periphery (Fig. 3). Thus, pO_2 values are generally higher than those found using the Eppendorf histograph in this tumor line. We note that the standard protocol for histography requires insertion of the electrode into the tumor (generally > 1.4 mm), before accepting readings. Here, the pO_2 values coincide with our own previous spectroscopic observations of the tumor periphery following direct i.t. injection (15, 16). The values also match those observed following i.v. administration of a perfluorocarbon emulsion, which tended to become sequestered in the well-perfused regions (23). Such regional differences draw attention to the need for a standard protocol for depositing HFB i.t., if the distribution of pO_2 values is to be fully representative of the whole tumor. Application of the histograph is based on many developmental sampling studies to define the minimum/optimal number of tracks and number of individual pO_2 measurements required (24–26). Moreover, interlaboratory comparison was performed to examine bias (27). We are now developing a standard protocol to ensure adequate representation of all tumor regions. Here, we have interrogated some poorly oxygenated regions, but the majority of the interrogated regions were well oxygenated. Significantly, this study has led to the observation that pO_2 may be manipulated in large tumors, at least in the well-perfused regions.

Relatively rapid changes in pO_2 were observed in initially well oxygenated tumor regions (Fig. 6), as also reported by others (16, 17, 28, 29). The high baseline values presumably reflect well-perfused regions, which, thus, responded rapidly to changes in vascular oxygenation. Nonetheless, changes in oxygenation were still relatively slow compared with the blood itself, which we have recently investigated using NIR (near infrared) spectroscopy of the AT1 tumor line (30). Initially less well-oxygenated regions responded much more slowly, although 2 of 3 regions shown in Fig. 6 did show a borderline increase in pO_2 after 32 min indicating distinct heterogeneity in tumor oxygen dynamics. In current studies, we are extending our breathing challenge schedules beyond the 32 min used here, to determine whether such borderline changes in pO_2 will become more significant. Such observations could be valuable in establishing optimal preirradiation breathing times for maximizing tumor pO_2 in the clinical setting. The range of response times emphasizes the importance of being able to map regional pO_2, because subtle local variations may be masked during global measurements. Ultimately, at least 90% of the tumor regions interrogated in this study showed an increase in pO_2 when the rats inhaled 100% oxygen. The linear regression analysis shows a less-clear trend than found previously (16, 18), but the Student's *t* test showed a significant increase in pO_2, even for those regions initially less than 15 torr. The heterogeneity in response emphasizes the importance of measuring dynamic changes, because baseline measurements do not directly predict the outcome of an intervention, and both acutely and chronically hypoxic regions are likely to be present.

Historically, it has been suggested that carbogen has a greater influence on tumor oxygenation than oxygen, and, indeed, carbogen has been used in adjuvant therapies with perfluorocarbon emulsions (31), and, more recently, as part of the ARCON (Accelerated Radiotherapy with CarbOgen and Nicotinamide) clinical trial (32). Our data suggest that oxygen and carbogen have a similar influence in the AT1 tumor (Figs. 8 and 9). However, further studies will be required to rigorously compare the two gases, because preconditioning by initially breathing oxygen may have influenced the results. The data are consistent with our previous spectroscopic investigations of individual tumor regions, which indicated that order of administration was unimportant, and that carbogen and oxygen had a similar influence on tumor oxygenation (16). Because changes were still occurring with either gas after 32 min, longer breathing times will ultimately need to be assessed.

In other animal studies, the influence of elevated oxygen concentrations or carbogen has been found highly tumor dependent. Thus, van der Sanden *et al.* found a significant rise in pO_2 in human glioma xenografts in nude mice with carbogen, but no change with oxygen (33). Brizel *et al.* (34) found no influence of normobaric oxygen ($FO_2 = 100\%$) or normobaric carbogen on the mammary adenocarcinoma R3230Ac implanted s.c., but hyperbaric oxygen and hyperbaric carbogen both caused significant changes. The same tumor implanted i.m. did show a response to normobaric carbogen (35). In a different laboratory, this tumor line was found to respond to normobaric carbogen when implanted s.c., but in the absence of mechanical ventilation (36). Other tumors have shown transient effects, with elevated pO_2 for some minutes, but ultimately return to baseline (37), emphasizing the need for measurements in each individual tumor in order to establish prognostic value.

Development of a new technique warrants comparison with other methods. Tumor oximetry techniques may be categorized by the degree of invasiveness and capacity to measure dynamic changes. NMR can be entirely noninvasive and early studies examined the phosphorylation potential based on ^{31}P NMR, but it is now recognized that this measures metabolic hypoxia, rather than radiobiological hypoxia (38). BOLD (blood oxygen level dependant) contrast proton NMR facilitates rapid interrogation of vascular oxygenation and is particularly appropriate for examining dynamic responses to interventions (39). However, BOLD

does not provide absolute pO_2 values and is confounded by the influence of blood flow, as investigated extensively by Howe *et al.* who termed the expression FLOOD (flow and oxygen level dependant) contrast (40). Although near infrared has traditionally been applied in conjunction with biopsy and cryospectrophotometry to interrogate vascular oxygenation (41), it may also be used noninvasively (30), but at this stage *in vivo* studies lack spatial resolution.

Direct pO_2 estimates have been achieved using static oxygen selective microelectrodes, which provided evidence for changes in regional pO_2 with elevated inhaled oxygen (28, 29). Recently, a fiber optic device (OxyLite™) has also shown promise for measuring dynamic changes in pO_2 (42). Although such methods are cheap, they are generally limited to sampling a few locations. Moving such a device through a tumor enables the distribution of pO_2 to be established, e.g., across one or more tracks to produce profiles or maps (24). The baseline distributions of pO_2 values obtained by such techniques have been shown to have clinical prognostic value in advanced cervical cancers (1, 2), head-and-neck sarcomas (4) and possibly breast tumors (43). This approach is less satisfactory for examining dynamic changes, however, because parallel tumor regions must be interrogated.

To avoid violating a tumor, molecular indicators have been developed for i.v. or i.p. administration. These have been applied to examine vascular oxygenation soon after administration based on phosphorescence (44) or ^{19}F NMR (45). The fluorocarbon approach has also been applied following clearance from the vasculature and sequestration in tissue (23, 46–49). However, there is increasing evidence that such an approach biases measurements towards the well perfused regions, generally found at the tumor periphery (23, 46, 49). Furthermore, particulate indicators tend to show extensive uptake by the reticuloendothelial system, but relatively little accumulation in tumors, precluding efficient imaging (46, 50).

An alternative approach is the use of bio-reducible hypoxia markers such as nitroimidazoles, which have been shown to bind selectively to hypoxic tissues. Many variants have been proposed over the past 20 years and incorporation of radionuclides has facilitated noninvasive investigations using PET or SPECT, while ^{19}F labels permitted NMR spectroscopy (51, 52). At present, clinical trials require histological analysis of biopsies obtained 24 h following i.v. administration, precluding investigations of oxygen dynamics. However, pulse chase experiments with multiple indicators to assess response to interventions have been demonstrated in animals (53).

To interrogate specific regions of interest, oxygen sensitive reporter molecules have been introduced by direct i.t. injection. A number of reports have demonstrated successful application of electron spin resonance (ESR) to follow pO_2 sensitive indicators (54, 55). Although this work has been limited to single regions of interest per tumor, recent reports suggest that multivoxel ESR imaging is becoming feasible (56). We, and others, have now demonstrated the feasibility of ^{19}F MRI following i.t. injection of reporter molecules (17, 18, 49). In regard to i.t. administration, we favor very fine sharp needles (32 gauge) to minimize perturbation of the tumor architecture.

In the past, we have examined clearance and redistribution of HFB from tumors over a period of hours (15, 16). Hexafluorobenzene was found to clear with a typical half-life of about 10 h with minimal redistribution within the tumor (15). Stability of local pO_2 measurements under baseline conditions observed here (Fig. 6) and over longer periods observed previously (17), strongly suggests that regions of interrogation are constant. Hexafluorobenzene forms multiple discrete droplets within tissue and signal is typically observed from 5-10% of tumor volume (21). Whether this is the optimal volume requires further investigation.

The ultimate value of a new technique depends on its robustness and general feasibility. The indicator molecule HFB is cheap, and readily available, commercially. There is an extensive literature describing its remarkable lack of toxicity, teratogenicity, or mutagenicity (57–59), facilitating potential clinical application. More immediately, most small-animal NMR research systems can perform ^{19}F NMR studies, which exhibit high sensitivity, and essentially no background signal. Moreover, as other fluorinated indicators are developed, measurements may be combined with estimates of pH and metal ions (60). The single resonance makes HFB particularly efficient for imaging studies, while the high T1 sensitivity to changes in pO_2 and minimal response to temperature make its use highly practical.

In other recent studies, we have extended application of the FREDOM technique to interrogate pO_2 in breast tumors in the rat, with respect to respiratory challenge (30) and human lymphoma xenografts in SCID mice, with respect to antibody-directed infarction (61). Nonetheless, we continue to seek further enhancement of the FREDOM approach. Administering more HFB could improve the local SNR or allow a larger volume to be interrogated, but this would be more invasive. Temporal resolution could be shortened by using fewer relaxation delays. Indeed, we have previously demonstrated 1-s time resolution in a perfused heart, albeit with much reduced precision in pO_2 estimates (62). The data may also be enhanced by application of appropriate apodization filters, which could improve SNR without seriously degrading the spatial resolution. Further refinement of the technique should be feasible, but we believe that this approach already represents a useful new method for interrogating tumor oxygen dynamics. While the technique is currently limited to preclinical investigations of animal tumors, we are seeking IND (investigational new drug) approval for HFB to facilitate future clinical applications. The ability to map pO_2 in 8 min makes this technique a practical proposition for application to patients and the value of monitoring dynamic changes in tumor oxygenation has the potential to influence treatment strategies.

REFERENCES

1. Höckel M, Schlenger K, Aral B, *et al.* Association between tumor hypoxia and malignant progression in advanced cancer of the uterine cervix. *Cancer Res* 1996;56:4509–4515.
2. Fyles AW, Milosevic M, Wong R, *et al.* Oxygenation predicts radiation response and survival in patients with cervix cancer. *Radiother Oncol* 1998;48:149–156.
3. Nordsmark M, Overgaard M, Overgaard J. Pretreatment oxygenation predicts radiation response in advanced squamous cell carcinoma of head and neck. *Radiother Oncol* 1996;41: 31–39.
4. Brizel DM, Scully SP, Harrelson JM, *et al.* Tumor oxygenation predicts for the likelihood of distant metastases in human soft tissue sarcoma. *Cancer Res* 1996;56:941–943.
5. Hall EJ. The oxygen effect and reoxygenation. In: Hall EJ, editor. Radiobiology for the radiologist. 3rd ed. Philadelphia: JB Lippincott; 1988. p. 137–160.
6. Chapman JD, Stobbe CC, Arnfield MR, *et al.* Oxygen dependency of tumor cell killing *in vitro* by light activated photofrin II. *Radiat Res* 1991;126:73–79.
7. Teicher B, Lazo J, Sartorelli A. Classification of antineoplastic agents by their selective toxicities toward oxygenated and hypoxic tumor cells. *Cancer Res* 1981;41:73–81.
8. Dische S, Saunders MI, Sealy R, *et al.* Carcinoma of the cervix and the use of hyperbaric oxygen with radiotherapy: A report of a randomized controlled trial. *Radiother Oncol* 1999; 53:93–98.
9. Brown JM. The hypoxic cell: A target for selective cancer therapy. *Cancer Res* 1999;59:5863–5870.
10. Stratford IJ, Adams GE, Bremmer JCM, *et al.* Manipulation and exploitation of the tumour environment for therapeutic benefit. *Int J Radiat Biol* 1994;65:85–94.
11. Durand RE, Olive PL. Physiologic and cytotoxic effects of tirapazamine in tumor-bearing mice. *Radiat Oncol Invest* 1997;5:213–219.
12. Stone HB, Brown JM, Phillips T, *et al.* Oxygen in human tumors: correlations between methods of measurement and response to therapy. *Radiat Res* 1993;136:422–434.
13. Vaupel PW, Kelleher DK, Günderoth M. Tumor oxygenation. Stuttgart: Gustav Fischer Verlag; 1995.
14. Vaupel PW, Schlenger K, Knoop C, *et al.* Oxygenation of human tumors: Evaluation of tissue oxygen distribution in breast cancers by computerized O_2 tension measurements. *Cancer Res* 1991;51:3316–3322.
15. Mason RP, Rodbumrung W, Antich PP. Hexafluorobenzene: A sensitive ^{19}F NMR indicator of tumor oxygenation. *NMR Biomed* 1996;9:125–134.
16. Hunjan S, Mason RP, Constantinescu A, *et al.* Regional tumor oximetry: ^{19}F NMR spectroscopy of hexafluorobenzene. *Int J Radiat Oncol Biol Phys* 1998;40:161–171.
17. Le D, Mason RP, Hunjan S, *et al.* Regional tumor oxygen dynamics: ^{19}F PBSR EPI of hexafluorobenzene. *Magn Reson Imaging* 1997;15:971–981.
18. Mason RP, Constantinescu A, Hunjan S, *et al.* Regional tumor oxygenation and measurement of dynamic changes. *Radiat Res* 1999;152:239–249.
19. Barker BR, Mason RP, Bansal N, *et al.* Oxygen tension mapping by ^{19}F echo planar NMR imaging of sequestered perfluorocarbon. *JMRI* 1994;4:595–602.
20. Hahn EW, Peschke P, Mason RP, *et al.* Isolated tumor growth in a surgically formed skin pedicle in the rat: A new tumor model for NMR studies. *Magn Reson Imaging* 1993;11:1007–1017.
21. Mason RP, Hunjan S, Le D, *et al.* Regional tumor oxygen tension: Fluorine echo planar imaging of hexafluorobenzene reveals heterogeneity of dynamics. *Int J Radiat Oncol Biol Phys* 1998;42:747–750.
22. Eble MJ, Wenz F, Bachert KB, *et al.* Invasive pO_2 histography in Dunning prostate tumor R-3327-AT1 and R3327-HI: Correlation with ^{31}P-MR spectroscopy and in-vivo radiosensitivity. In: Vaupel PW, Kelleher DK, Günderoth M, editors. Tumor oxygenation. Stuttgart: Gustav Fischer; 1995. p. 95–105.
23. Mason RP, Antich PP, Babcock EE, *et al.* Non-invasive determination of tumor oxygen tension and local variation with growth. *Int J Radiat Oncol Biol Phys* 1994;29:95–103.
24. Thews O, Kelleher DK, Vaupel PW. pO_2-mapping of experimental rat tumors: visualization and statistical analysis. In: Vaupel PW, Kelleher DK, Günderoth M, editors. Tumor oxygenation. Stuttgart: Gustav Fischer; 1995. p. 27–38.
25. Wong RKW, Fyles A, Milosevic M, *et al.* Heterogeneity of polarographic oxygen tension measurements in cervix cancer: An evaluation of within and between tumor variability, probe position, and track depth. *Int J Radiat Oncol Biol Phys* 1997; 39:405–412.
26. Yeh KA, Biade S, Lanciano RM, *et al.* Polarographic needle electrode measurements of oxygen in rat prostate carcinomas: Accuracy and reproducibility. *Int J Radiat Oncol Biol Phys* 1995;33:111–118.
27. Nozue M, Lee I, Yuan F, *et al.* Interlaboratory variation in oxygen tension measurement by Eppendorf "Histograph" and comparison with hypoxic marker. *J Surg Oncol* 1997;66:30–38.
28. Cater D, Silver I. Quantitative measurements of oxygen tension in normal tissues and in the tumors of patients before and after radiotherapy. *Acta Radiol* 1960;53:233–256.
29. Vaupel P. Atemgaswechsel und Glucosestoffwechsel von Implantationstumoren (DS-Carcinosarkom) *in vivo*. Vol. 1. Mainz: Akademie der Wissenschaften und der Literatur; 1974 (Thews G, ed. Funktionsanalyse biologischer Systeme).
30. Worden KL, Song Y, Jiang X, *et al.* Tumor oximetry: A comparison between near-infrared frequency domain spectroscopy of hemoglobin saturation and ^{19}F MRI of hexafluorobenzene. SPIE Conference on Optical Tomography and Spectroscopy of Tissue 111, San Jose, CA:1999. p. 601–610.
31. Teicher BA. Physiologic mechanisms of therapeutic resistance. *Hematol Oncol Clin North Am* 1995;9:475–506.
32. Kaanders JHAM, Pop LAM, Marres HAM, *et al.* Accelerated radiotherapy with carbogen and nicotinamide (ARCON) for laryngeal cancer,. *Radiother Oncol* 1998;48:115–122.
33. van der Sanden BJP, Heerschap A, Hoofd L, *et al.* Effect of carbogen breathing on the physiological profile of human glioma xenografts. *Magn Reson Med* 1999;42:490–499.
34. Brizel DM, Lin S, Johnson JL, *et al.* The mechanisms by which hyperbaric oxygen and carbogen improve tumour oxygenation. *Br J Cancer* 1995;72:1120–1124.
35. Lanzen JL, Braun RD, Ong AL, *et al.* Variability in blood flow and pO_2 in tumors in response to carbogen breathing. *Int J Radiat Oncol Biol Phys* 1998;42:855–859.
36. Al-Hallaq HA, River JN, Zamora M, *et al.* Correlation of magnetic resonance and oxygen microelectrode measurements of carbogen-induced changes in tumor oxygenation. *Int J Radiat Oncol Biol Phys* 1998;41:151–159.
37. Falk S, Ward R, Bleehen N. The influence of carbogen breathing on tumor tissue oxygenation in man evaluated by computerized pO_2 histography. *Br J Cancer* 1992;66:919–924.
38. Vaupel P, Kelleher DK, Engel T. Stable bioenergetic status despite substantial changes in blood flow and tissue oxygenation in a rat tumour. *Br J Cancer* 1994;69:46–49.
39. Robinson SP, Howe FA, Rodrigues LM, *et al.* Magnetic resonance imaging techniques for monitoring changes in tumor oxygenation and blood flow. *Semin Radiat Oncol* 1998; 8:198–207.

40. Howe FA, Robinson SP, Rodrigues LM, *et al.* Flow and oxygenation dependent (FLOOD) contrast MR imaging to monitor the response of rat tumors to carbogen breathing. *Magn Reson Imaging* 1999;17:1307–1318.
41. Fenton BM, Paoni SF, Lee J, *et al.* Quantification of tumour vasculature and hypoxia by immunohistochemical staining and HbO_2 saturation measurements. *Br J Cancer* 1999;79: 464–471.
42. Mason RP, Zhao D, Constantinescu A, *et al.* Tumor oximetry: Comparison of ^{19}F MR EPI (FREDOM) and the fiber-optic OxyLite™ (Abstr.). Denver:ISMRM; 2000. p. 1040.
43. Vaupel P, Hockel M. Oxygenation status of breast cancer: The Mainz experience. In: Vaupel P, Kelleher DK, editors. Tumor hypoxia. Stuttgart: Wissenschaftliche Verlagsgesellschaft; 1999. p. 1–11.
44. Vinogradov SA, Lo L-W, Jenkins WT, *et al.* Noninvasive imaging of the distribution of oxygen in tissues *in vivo* using near-infrared phosphors. *Biophys J* 1996;70:1609–1617.
45. Fishman JE, Joseph PM, Carvlin MJ, *et al. In vivo* measurements of vascular oxygen tension in tumors using MRI of a fluorinated blood substitute. *Invest Radiol* 1989;24:65–71.
46. van der Sanden BPJ, Heerschap A, Simonetti AW, *et al.* Characterization and validation of non-invasive oxygen tension measurements in human glioma xenografts by 19F-MR relaxometry. *Int J Radiat Oncol Biol Phys* 1999;44:649–658.
47. Dardzinski BJ, Sotak CH. Rapid tissue oxygen tension mapping using ^{19}F Inversion-recovery echo-planar imaging of Perfluoro-15-crown-5-ether. *Magn Reson Med* 1994;32:88–97.
48. Baldwin NJ, Ng TC. Oxygenation and metabolic status of KHT tumors as measured simultaneously by ^{19}F magnetic resonance imaging and ^{31}P magnetic resonance spectroscopy. *Magn Reson Imaging* 1996;14:514–551.
49. McIntyre DJO, McCoy CL, Griffiths JR. Tumour oxygenation measurements by ^{19}F MRI of perfluorocarbons. *Curr Sci* 1999;76:753–762.
50. Mason RP, Antich PP, Babcock EE, *et al.* Perfluorocarbon imaging *in vivo*: A ^{19}F MRI study in tumor-bearing mice. *Magn Reson Imaging* 1989;7:475–485.
51. Hodgkiss RJ. Use of 2-nitroimidazoles as bioreductive markers for tumour hypoxia. *Anticancer Drug Des* 1998;13:687–702.
52. Chapman JD, Engelhardt EL, Stobbe CC, *et al.* Measuring hypoxia and predicting tumor radioresistance with nuclear medicine assays. *Radiother Oncol* 1998;46:229–237.
53. Bussink J, Strik AM, Ljungkvist ASE, *et al.* Measurement and modification of oxygenation in human tumor xenografts (Abstr.). 47th Annual Meeting of Radiation Research Society, Albuquerque, NM, 2000. p. 96.
54. O'Hara JA, Goda F, Demidenko E, *et al.* Effect on regrowth delay in a murine tumor of scheduling split-dose irradiation based on direct pO_2 measurements by electron paramagnetic resonance oximetry. *Radiat Res* 1998;150:549–556.
55. Goda F, O'Hara JA, Rhodes ES, *et al.* Changes of oxygen tension in experimental tumors after a single dose of X-ray irradiation. *Cancer Res* 1995;55:2249–2252.
56. Kuppusamy P, Afeworki R, Shankar RA, *et al.* In vivo electron paramagnetic resonance imaging of tumor heterogeneity and oxygenation in a murine model. *Cancer Res* 1998;58: 1562–1568.
57. Grosman YS, Kapitonenko TA. Pharmacology and toxicology of hexafluorobenzene. *Izv Estestvennonauchu Inst Pevinsk* 1973;15:155–163.
58. Courtney KD, Andrews JE. Teratogenic evaluation and fetal deposition of hexabromobenzene (HBB) and hexafluorobenzene (HFB) in CD-1 mice. *J Environ Sci Health B* 1984;19: 83–94.
59. Mortelmanns KM. "*In vitro*" microbiological mutagenicity assays of eight fluorocarbon taggant samples. *Gov Rep Announce Index* (*US*) 1981;81:2555.
60. Mason RP. Transmembrane pH gradients *in vivo*: Measurements using fluorinated vitamin B6 derivatives. *Curr Med Chem* 1999;6:481–499.
61. Mason RP, Constantinescu A, Ran S, *et al.* Oxygenation in a human tumor xenograft: manipulation through respiratory challenge and anti-body directed infarction. In: Dunn JF, Swartz HM, editors. Oxygen transport to tissue. XXII. Proceedings of the 27th Annual Meeting of the International Society on Oxygen Transport to Tissue, 2001. In press.
62. Mason RP, Jeffrey FMH, Malloy CR, *et al.* A noninvasive assessment of myocardial oxygen tension: ^{19}F NMR spectroscopy of sequestered perfluorocarbon emulsion. *Magn Reson Med* 1992;27:310–317.